Supporting Information

Cu-based Bimetallic Catalysts for Electrocatalytic Oxidative Dehydrogenation of Furfural with Practical Rates

Hengzhou Liu,[a] Jiaqi Yu,[b] Yifu Chen,[a] Jungkuk Lee,[a] Wenyu Huang,[b] Wenzhen Li[a*]

Corresponding author: wzli@iastate.edu

[a] *Department of Chemical & Biological Engineering, Iowa State University, Ames, IA 50011, USA.*
[b] *Department of Chemistry, Iowa State University, Ames, IA 50011, USA.*

*Corresponding author: Wenzhen Li, Email: wzli@iastate.edu , ORCID: 0000-0002-1020-5187.

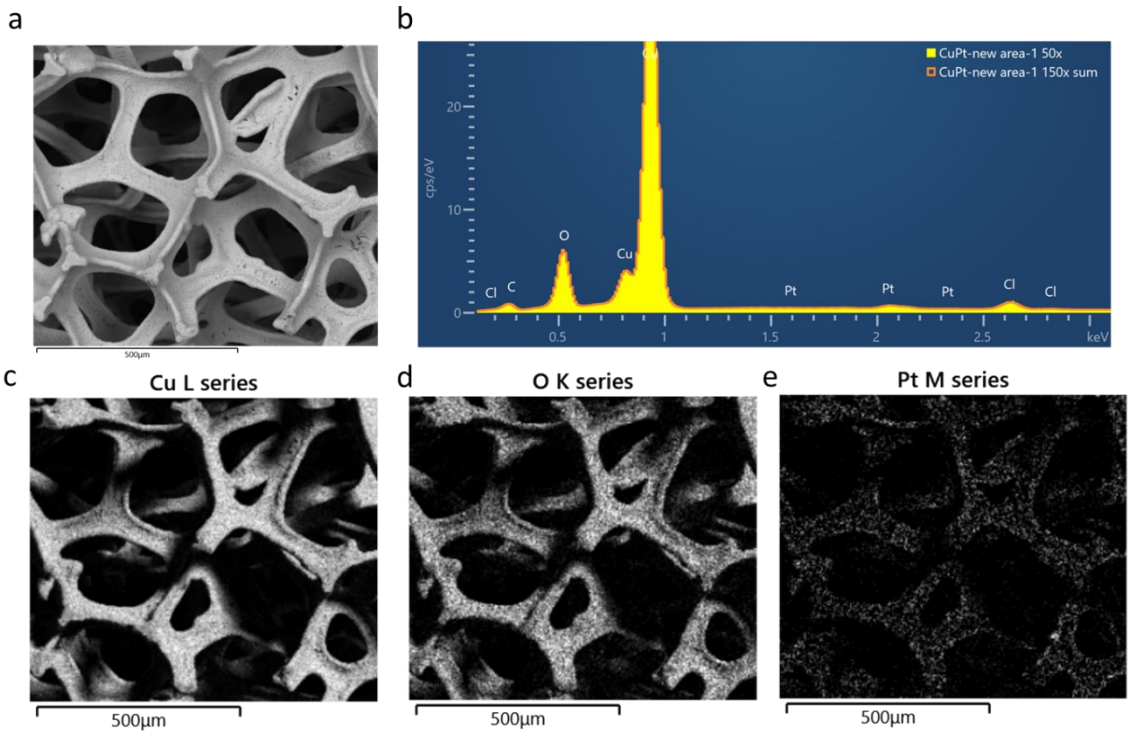

Figure S1. SEM-EDS of CuPt/Cu catalysts. (a) SEM image of CuPt/Cu electrode. (b) EDS of the entire region of (a). (c-e) The corresponding elemental mappings of Cu, O, and Pt.

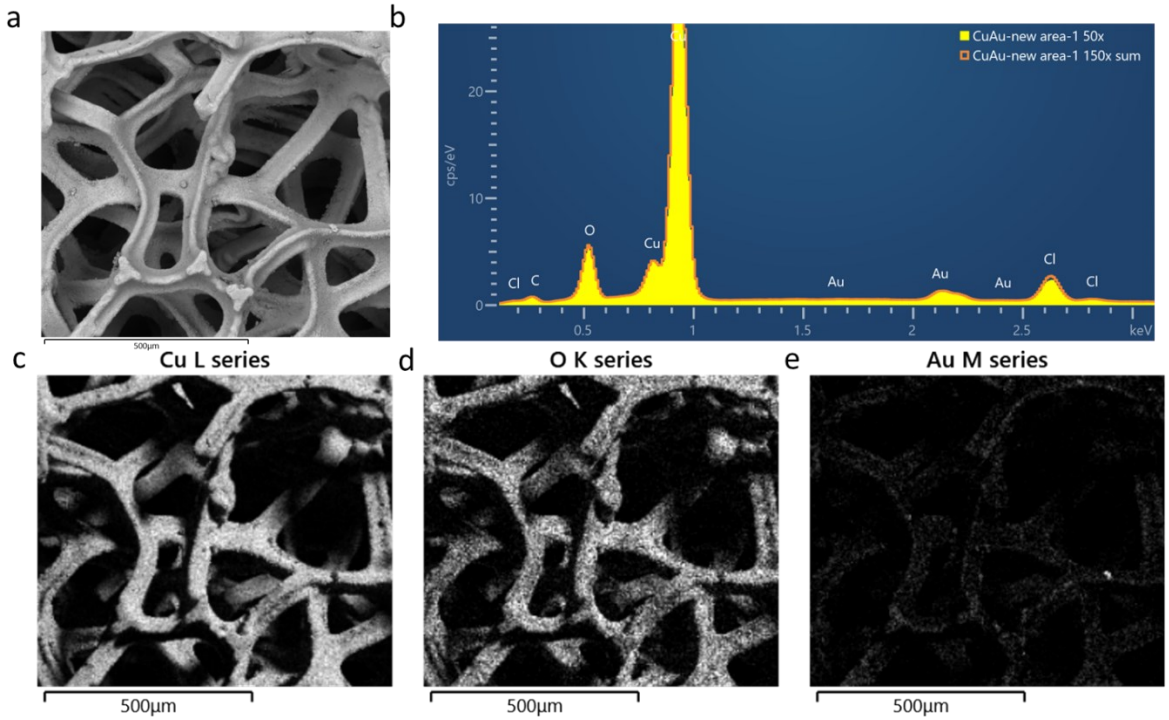

Figure S2. SEM-EDS of CuAu/Cu catalysts. (a) SEM image of CuAu/Cu electrode. (b) EDS of the entire region of (a). (c-e) The corresponding elemental mappings of Cu, O, and Au.

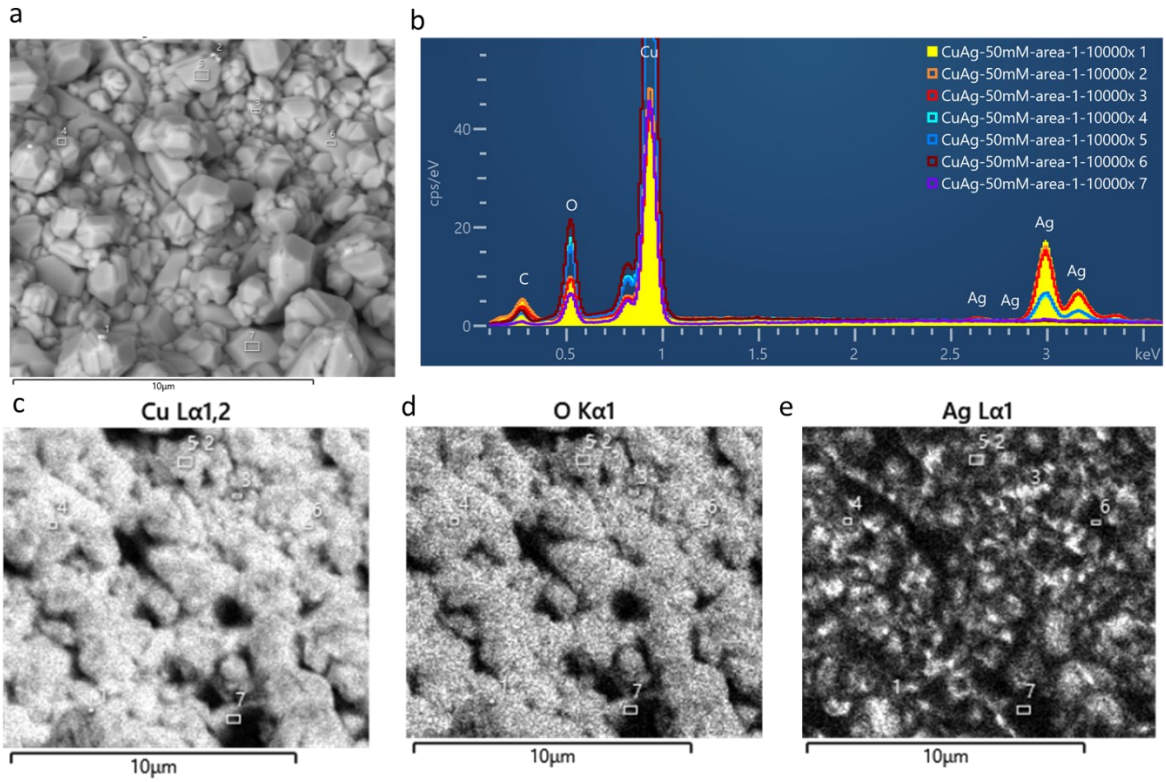

Figure S3. SEM-EDS of CuAg/Cu catalysts. (a) SEM image of CuAg/Cu electrode. (b) EDS of the entire region of (a). (c-e) The corresponding elemental mappings of Cu, O, and Ag. This data is adopted from our previous work.[1]

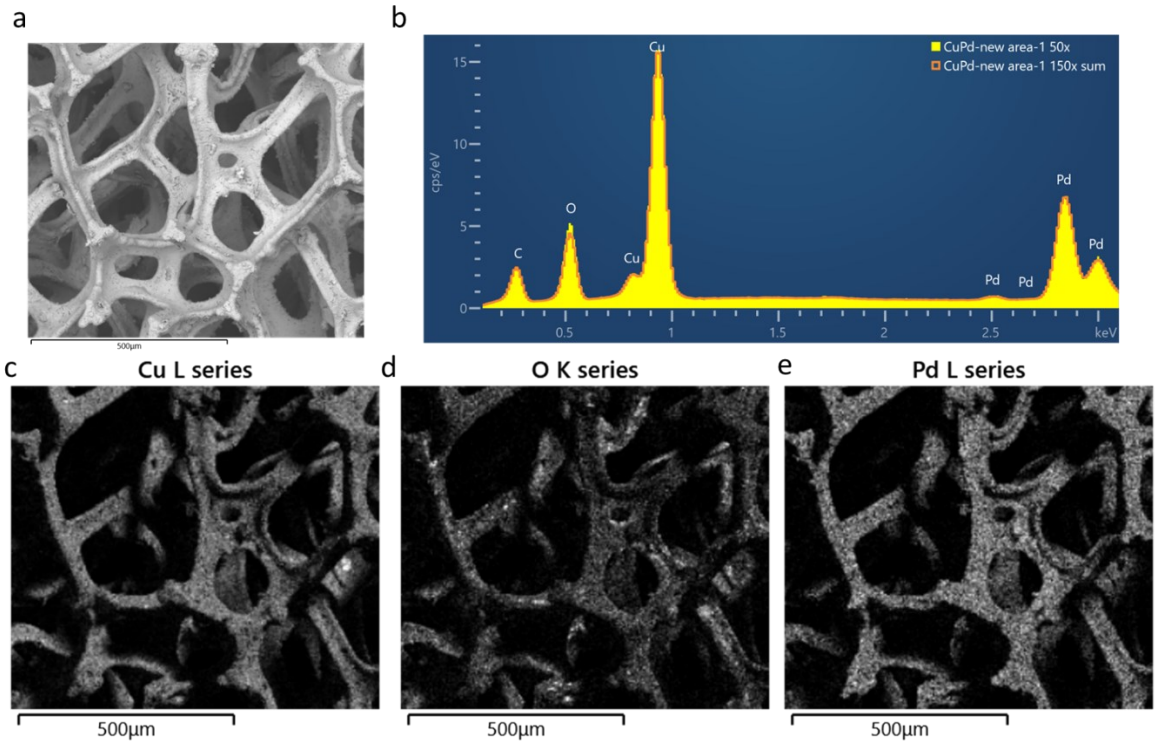

Figure S4. SEM-EDS of CuPd/Cu catalysts. (a) SEM image of CuPd/Cu electrode. (b) EDS of the entire region of (a). (c-e) The corresponding elemental mappings of Cu, O, and Pd.

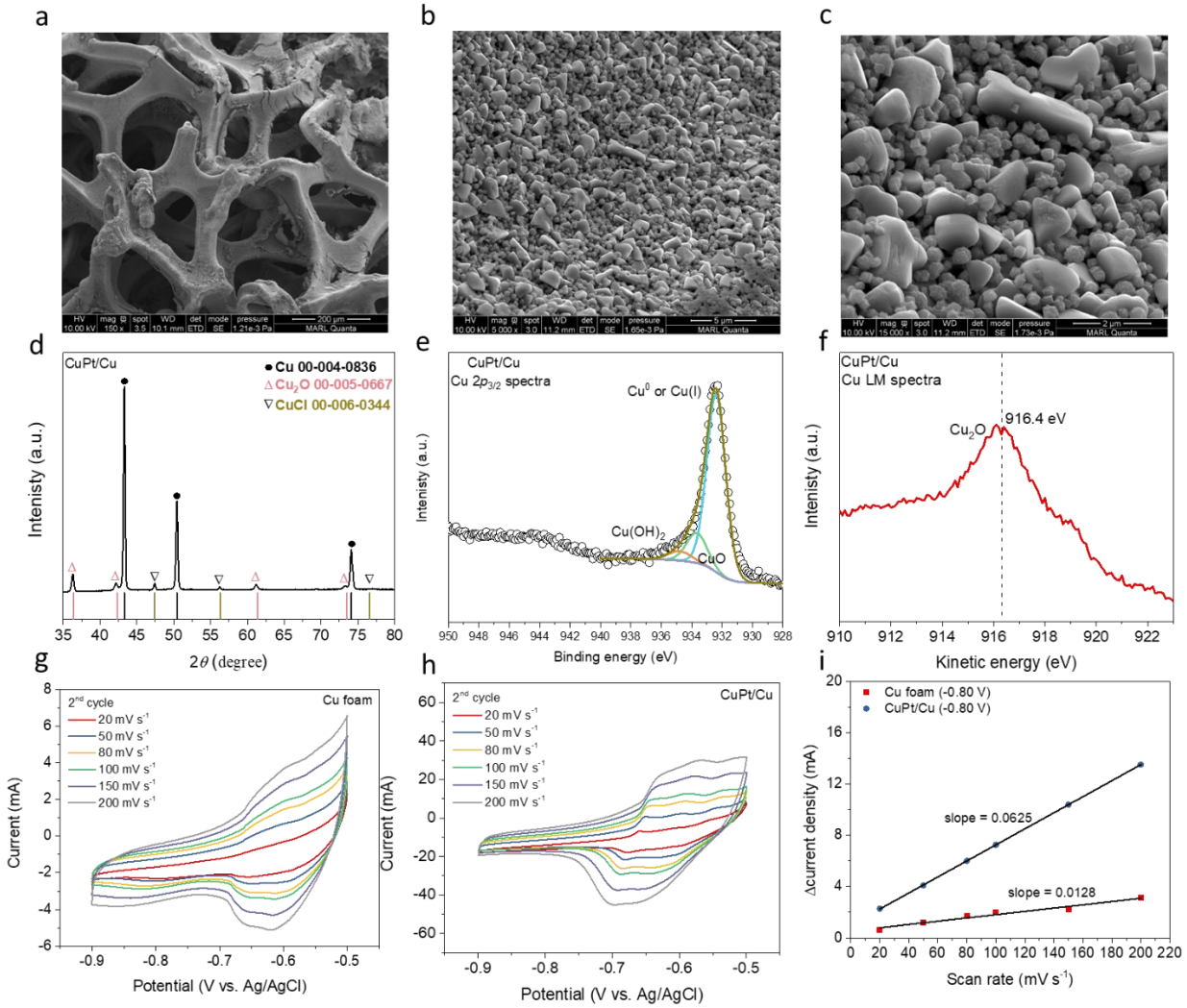

Figure S5. Characterization of CuPt/Cu catalysts. (a)-(c) SEM images. (d) XRD pattern. (e) XPS Cu $2p_{3/2}$ and (f) auger Cu LM spectra. (g)-(h) Cyclic voltammograms (CV, 2nd cycle) on Cu foam and CuPt/Cu. (i) Double-layer capacitance (C_{dl}), which was calculated on Cu-based electrodes at non-Faradaic regions (−0.80 V_{RHE}). The roughness factor of CuPt/Cu is 4.9, based on the slope normalization to Cu foam in (i).

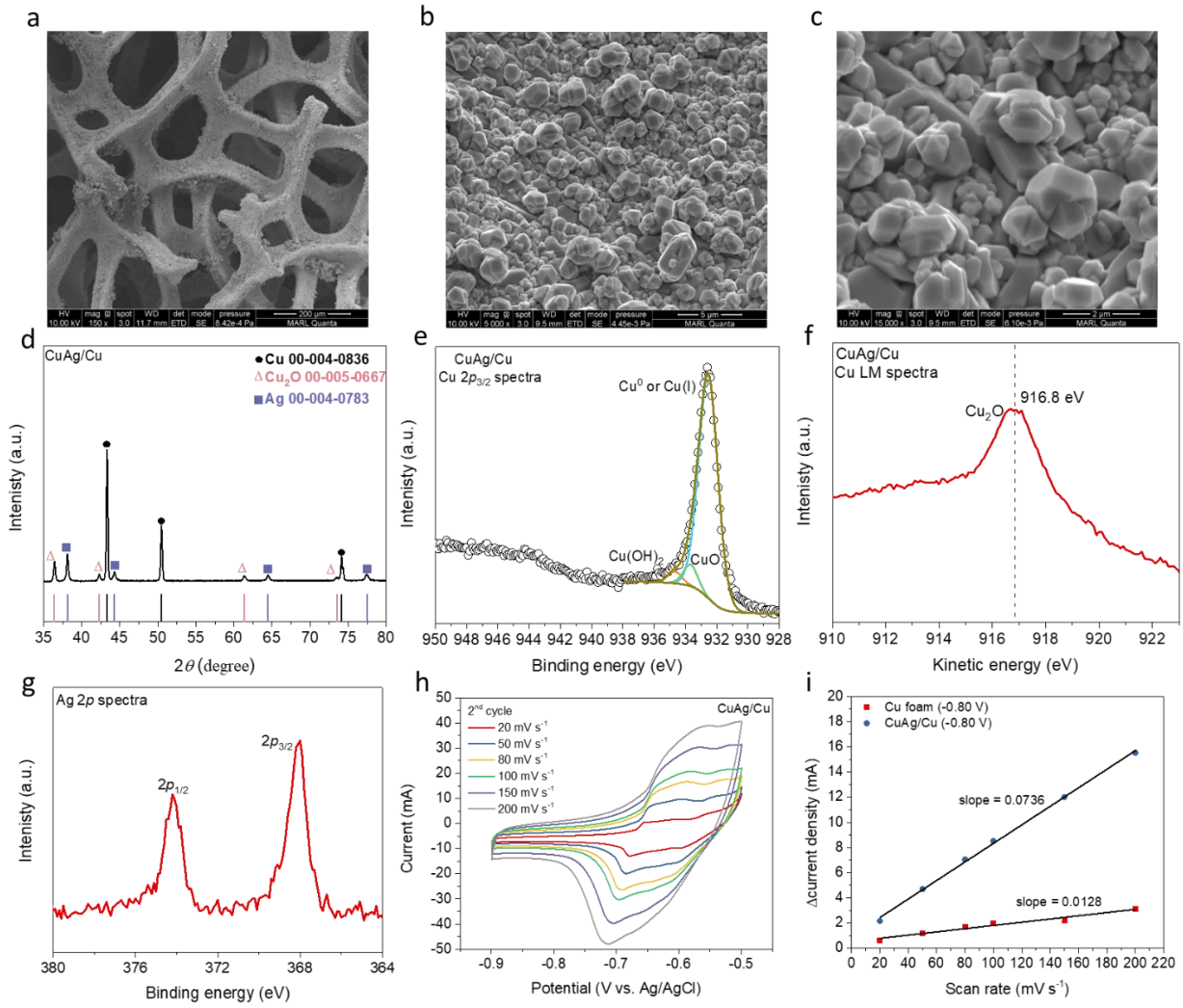

Figure S6. Characterization of CuAg/Cu catalysts. (a)-(c) SEM images. (d) XRD pattern. (e) XPS Cu $2p_{3/2}$, (f) auger Cu LM, and (g) Ag $2p$ spectra. (h)-(i) Cyclic voltammograms (CV, 2nd cycle) on Cu foam and CuPt/Cu. (i) Double-layer capacitance (C_{dl}), which was calculated on Cu-based electrodes at non-Faradaic regions (−0.80 V_{RHE}). The roughness factor of CuAg/Cu is 5.8, based on the slope normalization to Cu foam in (i).

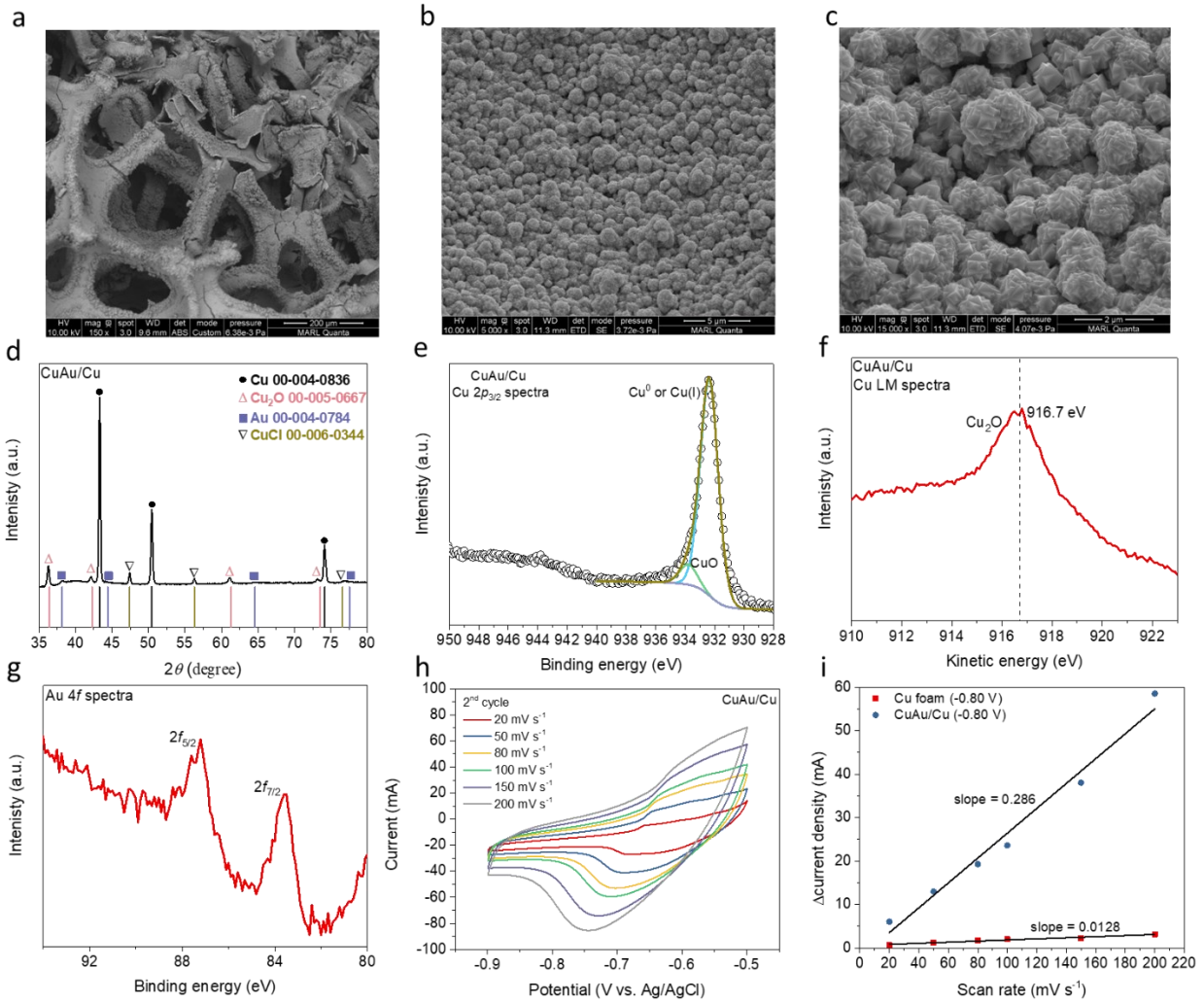

Figure S7. Characterization of CuAu/Cu catalysts. (a)-(c) SEM images. (d) XRD pattern. (e) XPS Cu $2p_{3/2}$, (f) auger Cu LM, and (g) Au 4*f* spectra. (h)-(i) Cyclic voltammograms (CV, 2nd cycle) on Cu foam and CuPt/Cu. (i) Double-layer capacitance (C_{dl}), which was calculated on Cu-based electrodes at non-Faradaic regions (−0.80 V_{RHE}). The roughness factor of CuAu/Cu is 22.3, based on the slope normalization to Cu foam in (i).

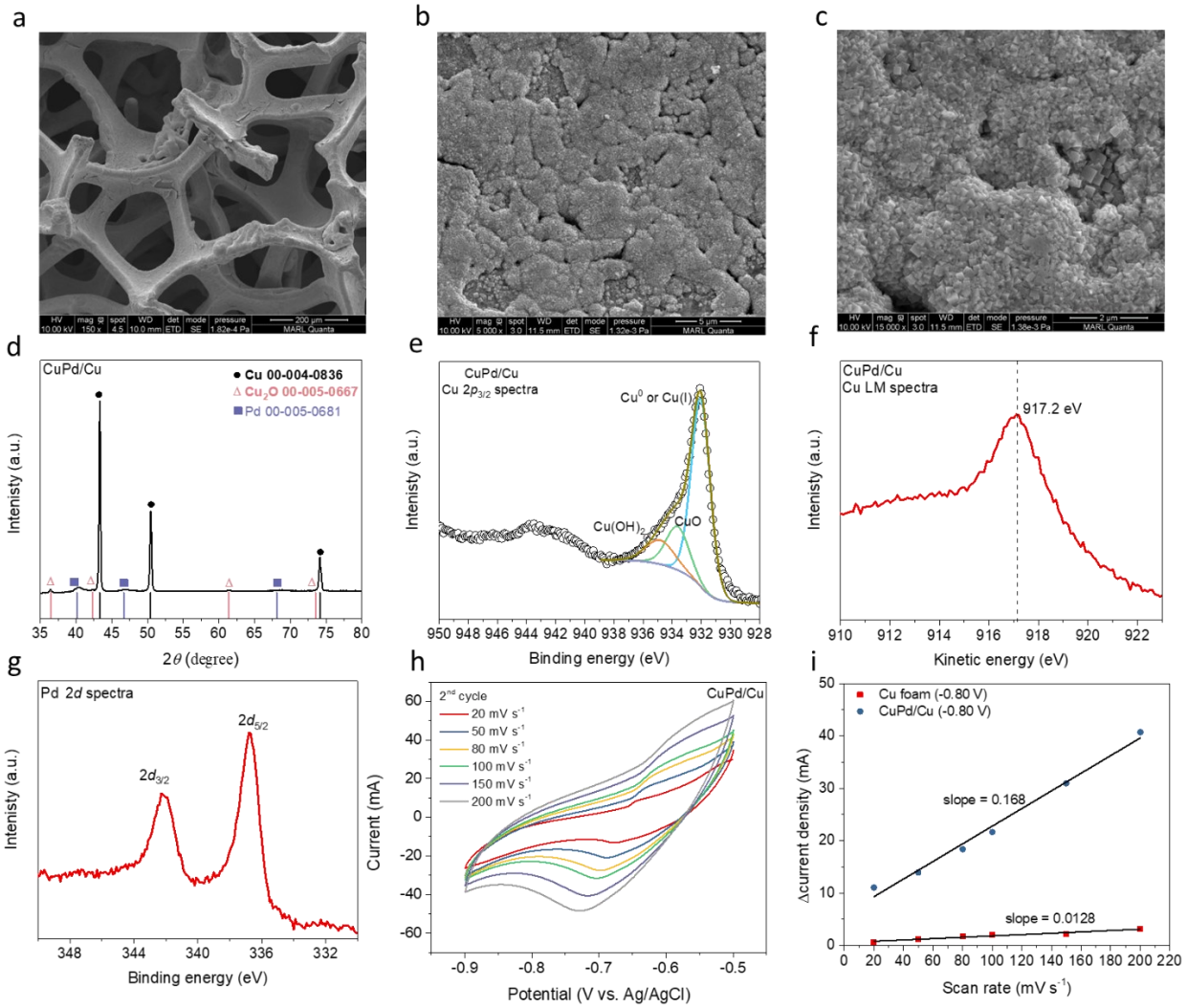

Figure S8. Characterization of CuPd/Cu catalysts. (a)-(c) SEM images. (d) XRD pattern. (e) XPS Cu $2p_{3/2}$, (f) auger Cu LM, and (g) Ag $2p$ spectra. (h)-(i) Cyclic voltammograms (CV, 2nd cycle) on Cu foam and CuPt/Cu. (i) Double-layer capacitance (C_{dl}), which was calculated on Cu-based electrodes at non-Faradaic regions (−0.80 V_{RHE}). The roughness factor of CuPd/Cu is 13.1, based on the slope normalization to Cu foam in (i).

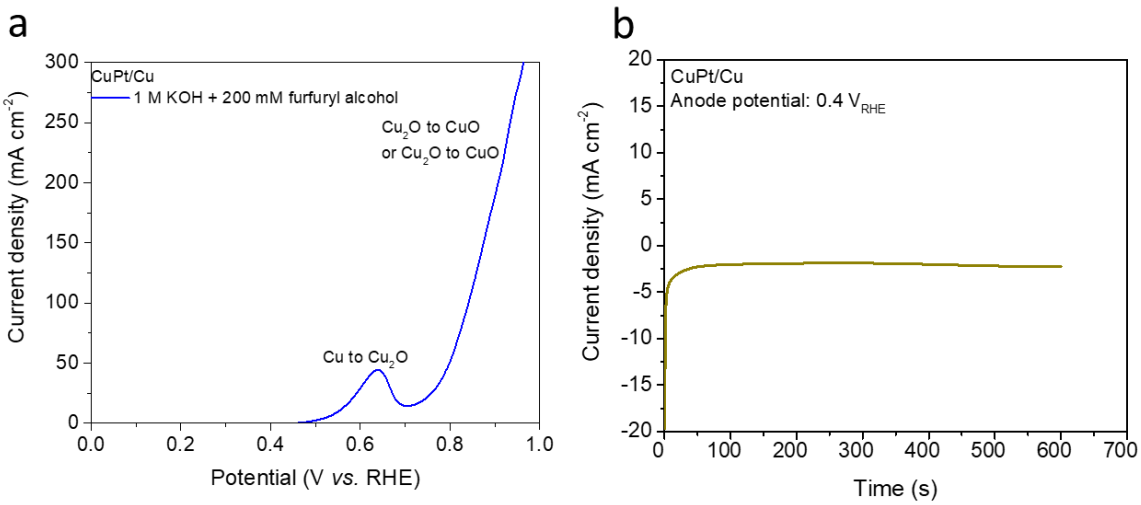

Figure S9. Control experiment of electrolysis with furfuryl alcohol on CuPt/Cu electrode. (a) LSV and (b) CA curves on $CuAg_{glv}$/Cu electrode. The current density at 0.4 V_{RHE} is due to the background double layer charging-discharging.

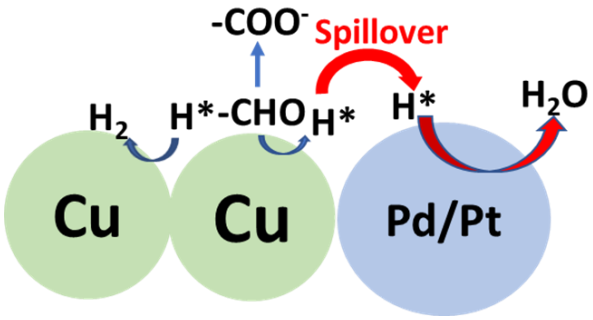

Figure S10. Hypothesized schematic illustration of a hydrogen spillover pathway on CuPd/Cu and CuPt/Cu electrodes. Similar hydrogen spillover mechanisms were reported in other electrochemical reactions by using bimetallic catalysts, such as hydrogen evolution reaction.[2]

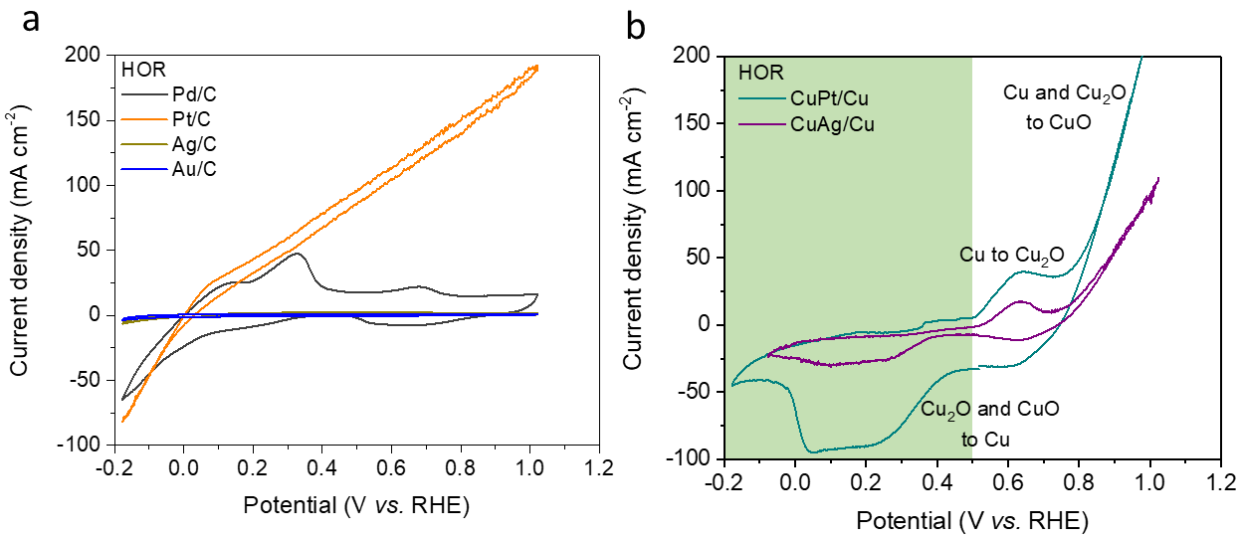

Figure S11. HOR on different catalysts. (a) HOR on commercial nanoparticles: Pt/C, Pd/C, Ag/C, and Au/C. (b) HOR on CuPt/Cu and CuAg/Cu electrodes. HOR was conducted in 1.0 M KOH with H_2 purging (100 mL min^{-1}).

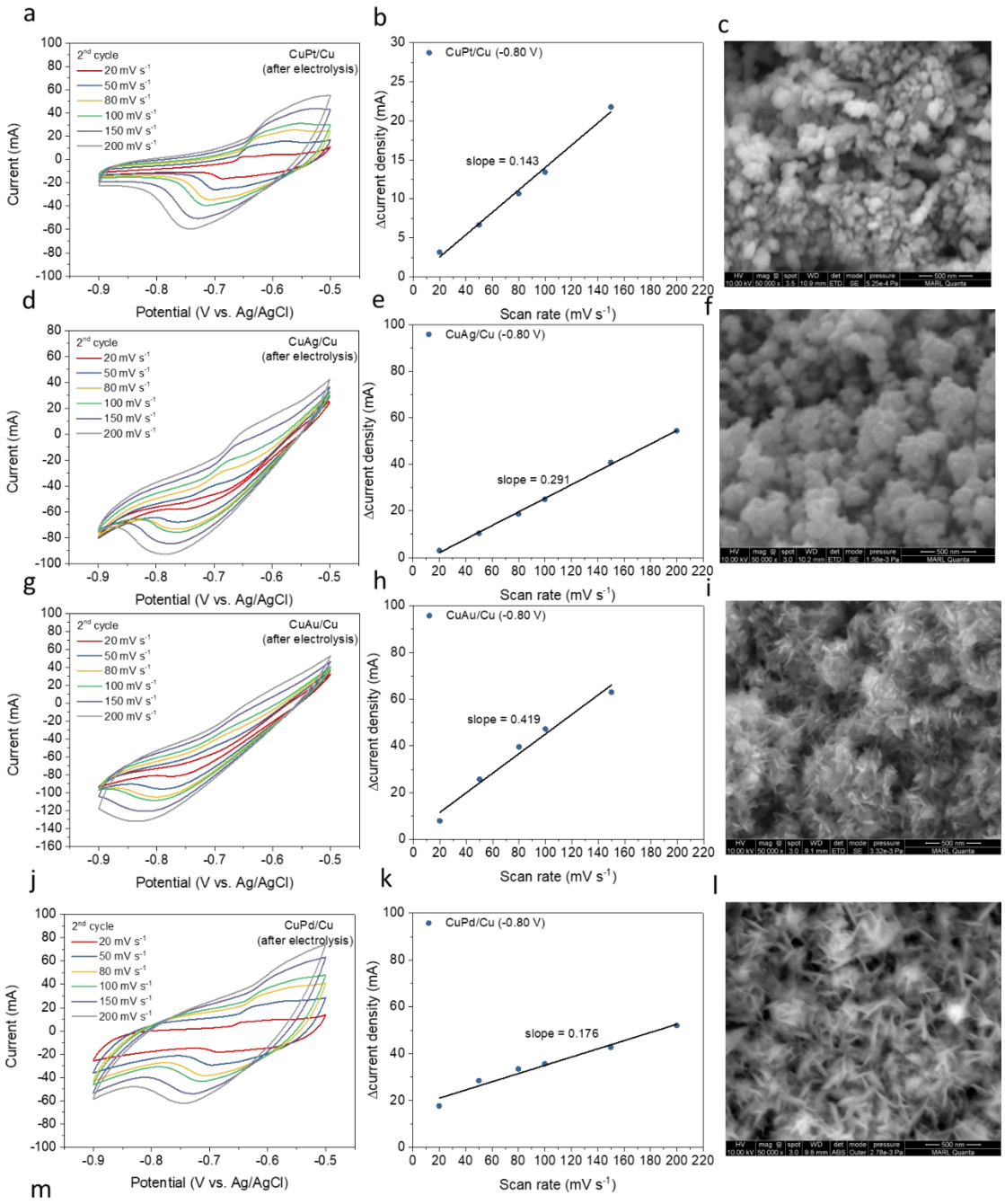

m

	CuPt/Cu	CuAg/Cu	CuAu/Cu	CuPd/Cu
Before electrolysis	4.9	5.8	22.3	13.1
After electrolysis	11.2	22.7	32.7	13.8

Figure S12. Characterization of Cu-based bimetals post-electrolysis. (a)-(l) Cyclic voltammograms (CV, 2nd cycle), double-layer capacitance (C_{dl}), and SEM images on CuM/Cu electrodes: CuPt/Cu, CuAg/Cu, CuAu/Cu, and CuPd/Cu. (m) Summary of the roughness factors before and after electrolysis. The electrolysis was conduced at 0.2 V_{RHE} for half-hour.

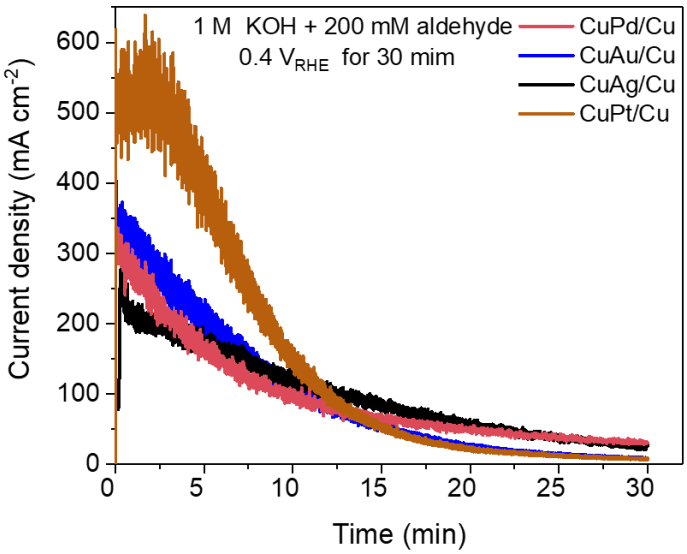

Figure S13. Current density – time profiles of half-hour electrolysis on four kinds of bimetals.

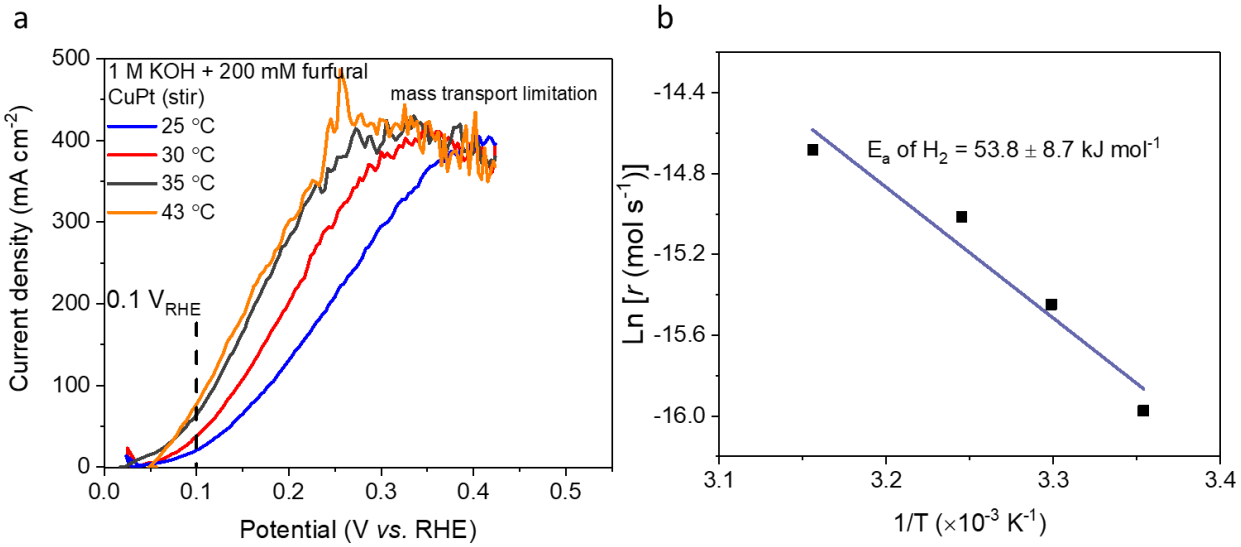

Figure S14. Activation energy for EOD on CuPt/Cu at 0.1 V_{RHE}. (a) Linear sweep voltammograms of CuPt/Cu in 1.0 M KOH with 200 mM furfural at different temperatures. The geometric area of CuPt/Cu was 1 cm^2. (b) Arrhenius plot for EOD on CuPt/Cu at 0.1 V_{RHE}.

a

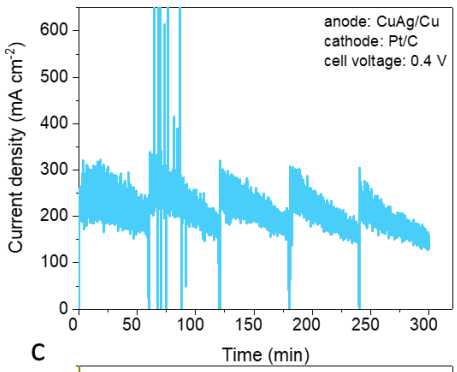

b

1-hour cycles on CuAg/Cu	Current density (mA cm^{-2})	Activity decrease percentrage (%)
1st	224	
2nd	226	-0.9
3rd	212	6.2
4th	203	4.2
5th	184	9.4

c

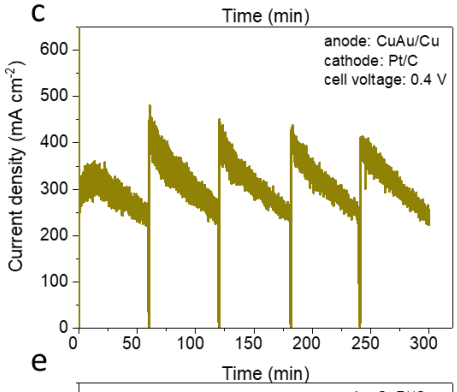

d

1-hour cycles on CuAu/Cu	Current density (mA cm^{-2})	Activity decrease percentrage (%)
1st	287	
2nd	317	-10.7
3rd	311	2.0
4th	307	1.3
5th	308	-0.3

e

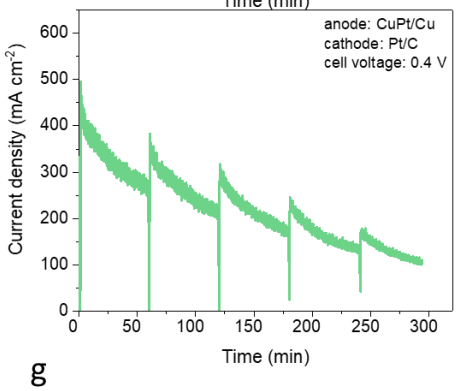

f

1-hour cycles on CuPt/Cu	Current density (mA cm^{-2})	Activity decrease percentrage (%)
1st	321	
2nd	261	18.6
3rd	214	18.1
4th	166	22.6
5th	126	23.8

g

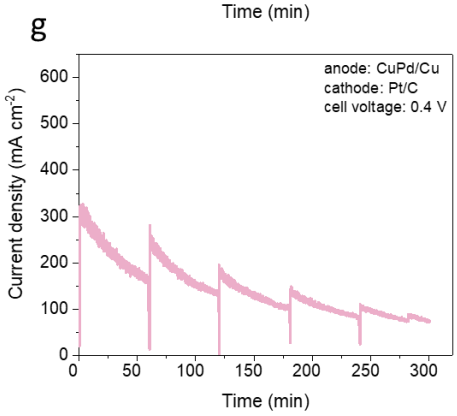

h

1-hour cycles on CuPd/Cu	Current density (mA cm^{-2})	Activity decrease percentrage (%)
1st	222	
2nd	175	21.4
3rd	133	24.4
4th	104	21.2
5th	85	18.3

Figure S15. Durability tests in the MEA-based flow cell with four kinds of Cu-based bimetals as anode: (a)-(b) CuAg/Cu; (c)-(d) CuAu/Cu; (e)-(f) CuPt/Cu; (g)-(h) CuPd/Cu. The current density – time profiles, and the summary of current density and activity decrease in each

1-hour cycle were shown in this Figure. The activity decrease percencentage is calculated by the equation, as follows:

$$\text{Activity decrease percentage} = \frac{i_n}{i_{n-1}}$$

Where i_n and i_{n-1} are the current densities at the n and n-1 cycle of 1-hour electrolysis.

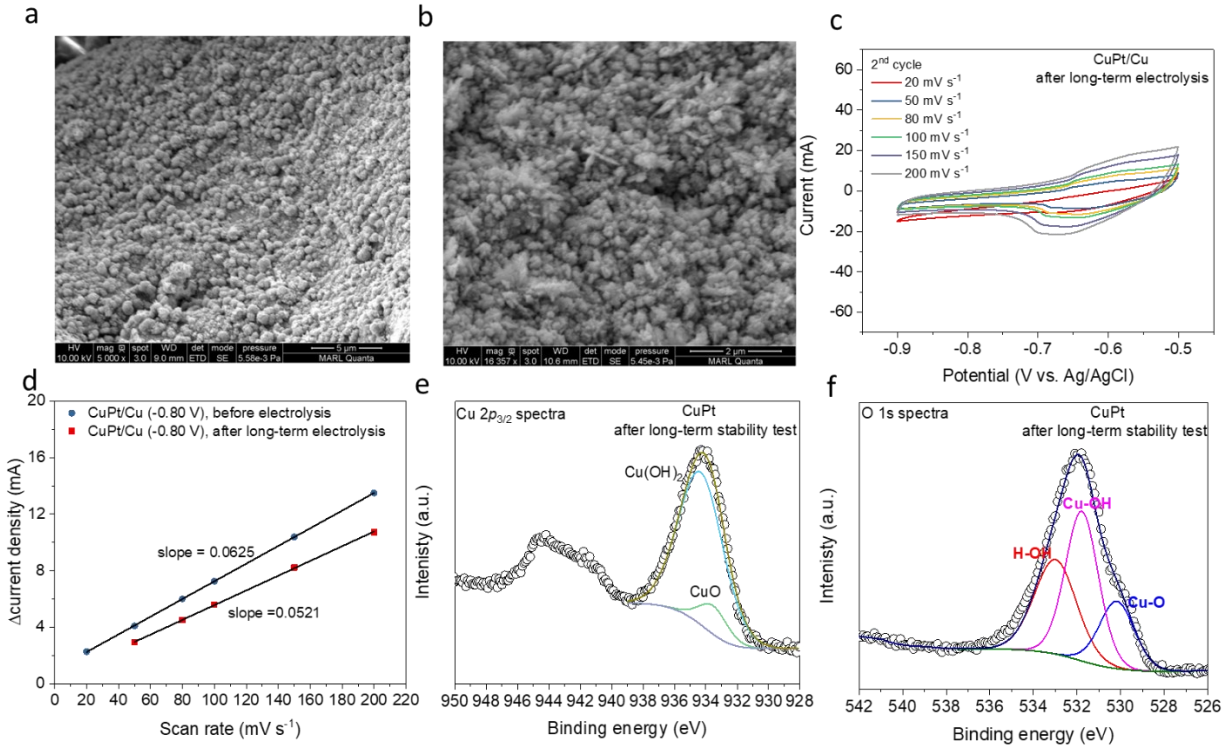

Figure S16. Physical characterization of CuPt/Cu electrode after long-term electrolysis. (a)-(b) SEM images. (c)-(d) Cyclic voltammograms (CV, 2nd cycle) and double-layer capacitance (C_{dl}) on CuPt/Cu electrode. (e) XPS Cu $2p_{3/2}$ and O1s spectra of CuPt/Cu electrode after long-term electrolysis of 5 cycles of 1-hour tests.

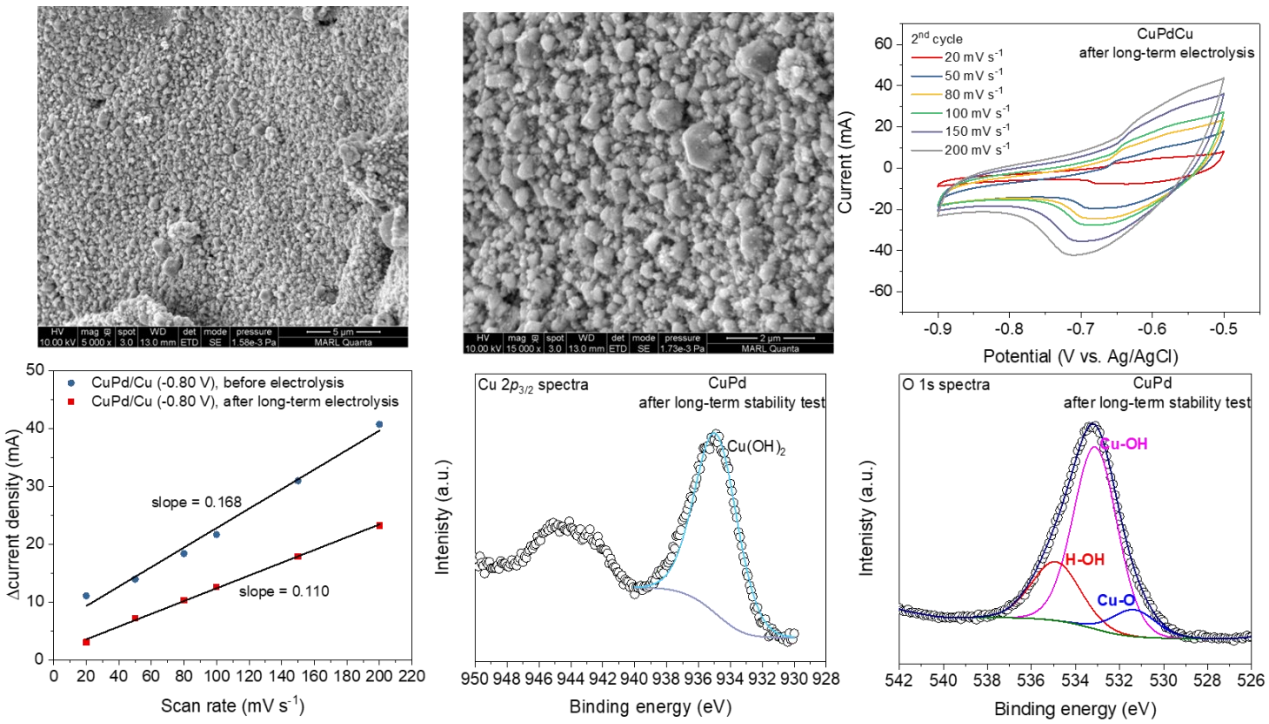

Figure S17. Physical characterization of CuPd/Cu electrode after long-term electrolysis. (a)-(b) SEM images. (c)-(d) Cyclic voltammograms (CV, 2nd cycle) and double-layer capacitance (C_{dl}) on CuPt/Cu electrode. (e) XPS Cu $2p_{3/2}$ and O1s spectra of CuPd/Cu electrode after long-term electrolysis of 5 cycles of 1-hour tests.

Table S1. Calculation of EOD reaction on CuM/Cu electrodes at 0.2 V_{RHE} for half-hour electrolysis.

Anode	Charge (C)	furfuryl alcohol (mM)	Total furoic acid (mM)	EOD-produced furoic acid (mM) [a]	FE of furoic acid from EOD (%)	Conversion (%) [b]
CuAg/Cu	103.8	20.4	119.6	99.2	112.8	65.4
CuAu/Cu	116.3	22.6	119.5	96.9	97.8	68.9
CuPd/Cu	161.9	20.1	145.0	124.9	93.4	70.3
CuPt/Cu	176.2	22.6	160.6	137.9	98.3	80.2

a. EOD-produced furoic acid = total furoic acid – Cannizzaro produced furoic acid (= quantified furfuryl alcohol).
b. The conversion of furfural in half-hour included three parts: Cannizzaro reaction, EOD reaction, and the degradation of furfural.

Table S2. Comparison of the EOD performance on various electrodes.

Anodic reactant	Anode	Anode product	j (mA cm^{-2})	Potential (V vs. RHE)	Ref.
furfural	Cu foam	furoic acid and H_2	100	0.31	[3]
	H-PdCu ANs		25	~0.60	[4]
	Pt-Cu		236	0.27	[5]
	$Cu(OH)_2$/Cu foam		100	0.40	[6]
	$CuAg_{gl\nu}$/Cu		209	0.40	[7]
	CuPt/Cu		357	0.40	This work
HCHO	Pd_{NP}/Pd	formic acid and H_2	28	0.5	[8]
	CF@Cu-NS		120	0.4	[9]

References

[1] H. Liu, N. Agrawal, A. Ganguly, Y. Chen, J. Lee, J. Yu, W. Huang, M.M. Wright, M. Janik, W. Li, Ultra-Low Voltage Bipolar Hydrogen Production from Biomass-Derived Aldehydes and Water in Membrane-Less Electrolyzers, Energy & Environmental Science, (2022).
[2] H.Q. Fu, M. Zhou, P.F. Liu, P. Liu, H. Yin, K.Z. Sun, H.G. Yang, M. Al-Mamun, P. Hu, H.-F. Wang, Hydrogen spillover-bridged Volmer/Tafel processes enabling ampere-level current density alkaline hydrogen evolution reaction under low overpotential, Journal of the American Chemical Society, 144 (2022) 6028-6039.
[3] T. Wang, L. Tao, X. Zhu, C. Chen, W. Chen, S. Du, Y. Zhou, B. Zhou, D. Wang, C. Xie, Combined anodic and cathodic hydrogen production from aldehyde oxidation and hydrogen evolution reaction, Nature Catalysis, (2021) 1-8.
[4] X. Zhang, T.-Y. Liu, Y. Zhou, L. Zhang, X.-C. Zhou, J.-J. Feng, A.-J. Wang, A transformative strategy to realize hydrogen production with electricity output through ultra-low potential furfural oxidation on hollow PdCu alloy networks, Applied Catalysis B: Environmental, 328 (2023) 122530.
[5] X. Zhang, W. Zhu, H. Zhou, L. Sun, Z. Wang, H. Liang, An Acid-Alkaline Furfural Hybrid Battery for Furoate and Bipolar Hydrogen Production, Chemical Communications, (2023).
[6] T. Wang, Z. Huang, T. Liu, L. Tao, J. Tian, K. Gu, X. Wei, P. Zhou, L. Gan, S. Du, Transforming electrocatalytic biomass upgrading and hydrogen production from electricity input to electricity output, Angewandte Chemie, 134 (2022) e202115636.
[7] H. Liu, N. Agrawal, A. Ganguly, Y. Chen, J. Lee, J. Yu, W. Huang, M.M. Wright, M.J. Janik, W. Li, Ultra-low voltage bipolar hydrogen production from biomass-derived aldehydes and water in membrane-less electrolyzers, Energy & Environmental Science, 15 (2022) 4175-4189.
[8] G. Li, G. Han, L. Wang, X. Cui, N.K. Moehring, P.R. Kidambi, D.-e. Jiang, Y. Sun, Dual hydrogen production from electrocatalytic water reduction coupled with formaldehyde oxidation via a copper-silver electrocatalyst, Nature Communications, 14 (2023) 525.
[9] Y. Yang, X. Wu, M. Ahmad, F. Si, S. Chen, C. Liu, Y. Zhang, L. Wang, J. Zhang, J.-L. Luo, A Direct Formaldehyde Fuel Cell for CO2-Emission Free Co-generation of Electrical Energy and Valuable Chemical/Hydrogen, Angewandte Chemie International Edition, (2023) e202302950.